

Fig. 4. Comparison of theoretical results of this paper with experimental results of Ragan [10] for a single, thick inductive iris with  $d = 23.8$  mm,  $d_i/d = 0.60$ , and  $f = 9.375$  GHz. The magnitude of the reflection coefficient is shown as a function of normalized iris thickness,  $t/d$ .

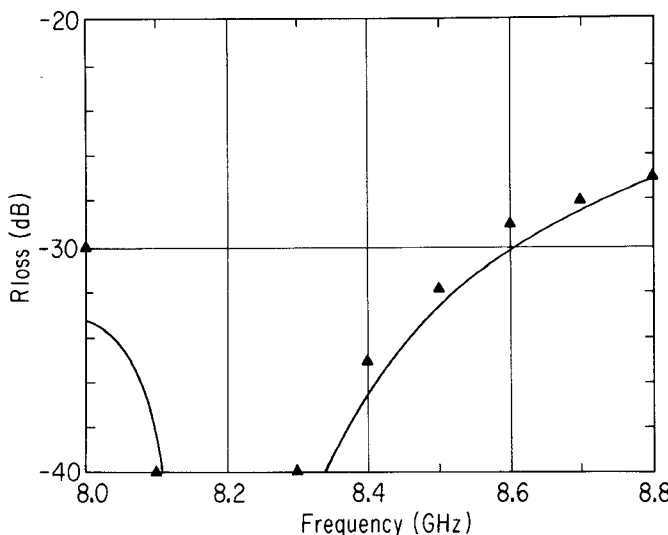


Fig. 5. Comparison of measured data with theory presented in this paper for a rexolite window with  $d = 1.02$  in,  $d_i = 0.855$  in,  $t = 0.025$  in, and  $t_i = 0.031$  in. The points represent the experiment, the curve, theory.

#### IV. VERIFICATION OF THEORY

For the cascade of circular waveguide step discontinuities there is a scarcity of data with which to compare. Ragan [10] presents some experimental results for the inductive iris in a circular waveguide. Ragan gives an equivalent circuit model with parameter values obtained from experimental results. He makes a comparison between the experimental data and theory for small holes in an infinitesimally thin iris. The results show that this theory has severe limitations when the size of the hole becomes large relative to the iris thickness. The iris consists of two step discontinuities, from left to right, a diameter reduction and diameter enlargement, separated by a homogeneous circular waveguide. Using the theory of the previous section, the two steps are modeled with generalized scattering matrices and then cascaded using the transmission matrix of the interconnecting circular

waveguide. The theoretical results, in the form of reflection coefficient, are found to be in excellent agreement with Ragan's experimental data, as shown in Fig. 4.

An experiment was carried out for a Rexolite ( $\epsilon_r = 2.54$ ) window with  $d = 1.02$  in,  $d_i = 0.855$  in,  $t = 0.025$  in, and  $t_i = 0.031$  in. The theoretical results show good agreement with experimental results, as shown in Fig. 5.

#### REFERENCES

- [1] A. Wexler, "Solution of waveguide discontinuities by modal analysis," *IEEE Trans. Microwave Theory Tech.*, vol. MTT-15, pp. 508-517, Sept. 1967
- [2] P. H. Masterman and P. J. B. Clarricoats, "Computer field-matching of waveguide transverse discontinuities," *Proc. Inst. Elec. Eng.*, vol. 118, no. 1, pp. 51-63, Jan. 1971
- [3] W. J. English, "The circular waveguide step-discontinuity mode transducer," *IEEE Trans. Microwave Theory Tech.*, vol. MTT-21, pp. 633-636, Oct. 1973
- [4] G. L. James, "Admittance of irises in coaxial and circular waveguides for  $TE_{11}$ -mode excitation," *IEEE Trans. Microwave Theory Tech.*, vol. MTT-35, pp. 430-434, Apr. 1987
- [5] H. Patzelt and F. Arndt, "Double-plane steps in rectangular waveguides and their application for transformers, irises, and filters," *IEEE Trans. Microwave Theory Tech.*, vol. MTT-30, pp. 771-776, May 1982
- [6] L. Carin, "Computational analysis of cascaded coaxial and circular waveguide discontinuities," Master's Thesis, Univ. of Maryland, College Park, 1986.
- [7] T. S. Chu and T. Itoh, "Generalized scattering matrix method for analysis of cascaded and offset microstrip step discontinuities," *IEEE Trans. Microwave Theory Tech.*, vol. MTT-34, pp. 280-284, Feb. 1986.
- [8] R. F. Harrington, *Time Harmonic Electromagnetic Fields*. New York: McGraw-Hill, 1961, ch. 8.
- [9] N. Marcuvitz, *Waveguide Handbook*. New York: McGraw-Hill, 1951, ch. 2.
- [10] G. L. Ragan, *Microwave Transmission Circuits*. New York: Dover, 1965, pp. 213-214.

#### A New Lock Indicator Circuit for Microwave and Millimeter-Wave Phase Locked Loops

JORDI BERENGUER I SAU, MEMBER, IEEE

**Abstract**—A new circuit useful as a lock detector in microwave PLL systems has been developed. This circuit avoids the quadrature phase detector or coherent amplitude detector commonly used as a lock indicator in PLL's, thereby reducing the microwave circuitry and components. It is based on the properties of the phase error signal coming from the phase detector; a frequency-voltage conversion is performed on it in a low-frequency (secondary) PLL, the input to which is the output of the phase detector in the main (microwave) PLL. The secondary VCO control signal gives, after a comparison, a logic level related to the lock condition in the main (microwave) PLL.

#### I. INTRODUCTION

In the development of microwave and millimeter-wave phase locked loops, where the phase detection is made at very high frequencies with conventional microwave mixers (analog multipliers), an indication of the lock condition requires the use of an additional phase detector where the VCO signal is fed through a  $90^\circ$  phase shifter (Fig. 1) [1]. This increases the system complex-

Manuscript received December 7, 1987; revised April 1, 1988. This work was supported by the Spanish National Commission for Science and Technology (C.A.Y.C.I.T.) under Grant 3346/83 and by the European Space Agency, with INISEL (Madrid) as main contractor.

The author is with the Dptmt. Teoria del Senyal i Comunicacions, E.T.S. Enginyers de Telecommunicació de Barcelona, Universitat Politècnica de Catalunya, Spain

IEEE Log Number 8822154

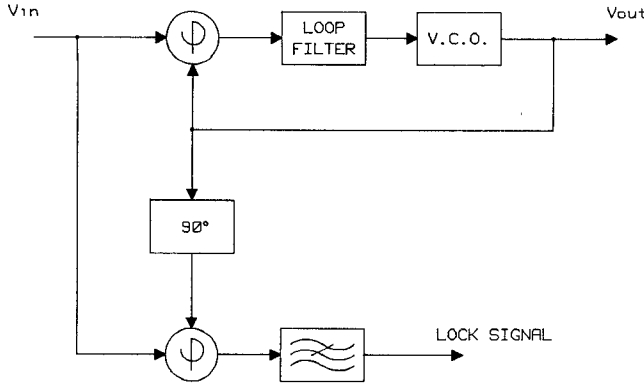


Fig. 1 Lock indicator system, using quadrature phase detector.

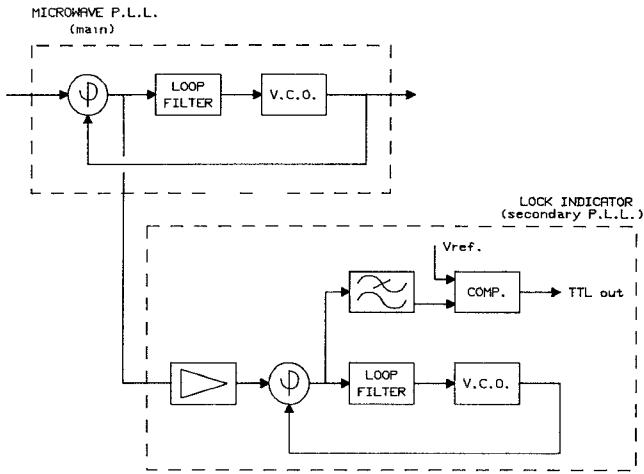


Fig. 2. Block diagram of the proposed lock indicator system

ity, size, and cost since it is not possible to use the common low-frequency integrated circuits which have this function included in the phase detector chip.

When the output signal of a PLL phase detector is displayed on a CRT, it is possible, by visual inspection, to check whether the PLL is locked or not; that is, the information about the lock condition is contained in this error signal, and the problem now is to extract this information from it with an electronic circuit.

The device presented here (Fig. 2) makes a frequency-voltage conversion of the phase detector output signal from the microwave (main) PLL in a secondary low-frequency PLL, which uses it as reference, thus giving with a logic level format an indication of the lock condition of the main PLL.

## II. THEORY OF OPERATION

The signal provided at the output of the main PLL phase detector is the phase error signal  $\Theta_e$  obtained by subtracting the VCO output signal phase  $\Theta_o$  from the input reference signal phase  $\Theta_i$ .

Under the lock condition, the linear model of the PLL, shown in Fig. 3, applies. From it, the following expression for the error signal can be obtained:

$$\Theta_e(s) = H_e(s)\Theta_i(s) = [1 - H(s)]\Theta_i(s)$$

with

$$H(s) = \frac{K_d K_v F(s)}{s + K_d K_v F(s)} \quad H_e(s) = \frac{s}{s + K_d K_v F(s)}$$

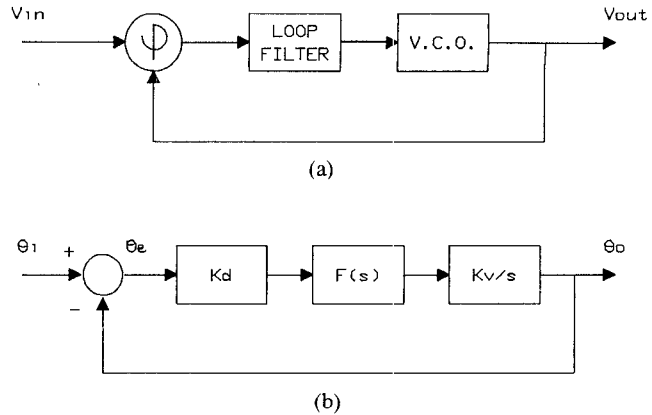


Fig. 3 PLL's block diagram. (a) Physical model. (b) Linearized model.

where  $F(s)$  is the loop filter transfer function,  $K_d$  is the phase detector constant (V/rad),  $K_v$  is the VCO constant (rad/s/V), and  $H(s)$  is the PLL transfer function, which has a low-pass behavior with a cutoff frequency  $B_n$ . As a consequence, the error signal  $\Theta_e$  is a high-pass filtered version of the reference  $\Theta_i$ .

Fig. 4(a) and (b) shows the plots of the squared modulus of the transfer functions  $H(s)$  and  $H_e(s)$  for a second-order PLL with loop filter transfer function  $F(s) = (1 + \tau_2 s)/s\tau_1$ , a cutoff frequency of 10 kHz, and a damping coefficient  $\zeta = 0.707$ . With the loop filter given above, the following expressions for  $H(s)$  and  $H_e(s)$  can be obtained:

$$H(s) = \omega_0^2 \frac{1 + 2\zeta s/\omega_n}{s^2 + 2\zeta\omega_n s + \omega_n^2}$$

$$H_e(s) = \frac{s^2}{s^2 + 2\zeta\omega_n s + \omega_n^2}$$

and

$$\tau_1 = \frac{K_d K_v}{\omega_n^2} \quad \tau_2 = \frac{2\zeta}{\omega_n}.$$

The power spectrum of the reference signal usually has a low-pass characteristic, with a roll-off in the passband [2]. A typical phase-noise plot of an X-band microwave oscillator is shown in Fig. 5(a). Therefore, the signal  $\Theta_e$  will be a bandpass noise signal peaked not far from the cutoff frequency  $B_n$ , with a bandwidth which depends on the spectrum of the reference signal and  $B_n$ .

Given that  $\theta_e(t)$  is a bandpass signal, it can be expressed as follows:

$$\theta_e(t) = A(t) \cos \varphi(t) = A(t) [\cos(\omega_0 t + \phi(t))]$$

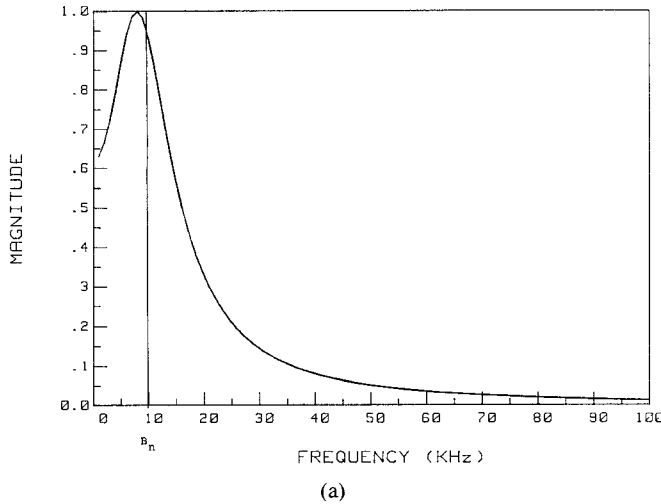
where the envelope  $A(t)$  and the instantaneous phase  $\varphi(t)$  are given by

$$A(t) = \sqrt{\theta_e^2(t) + \hat{\theta}_e^2(t)}$$

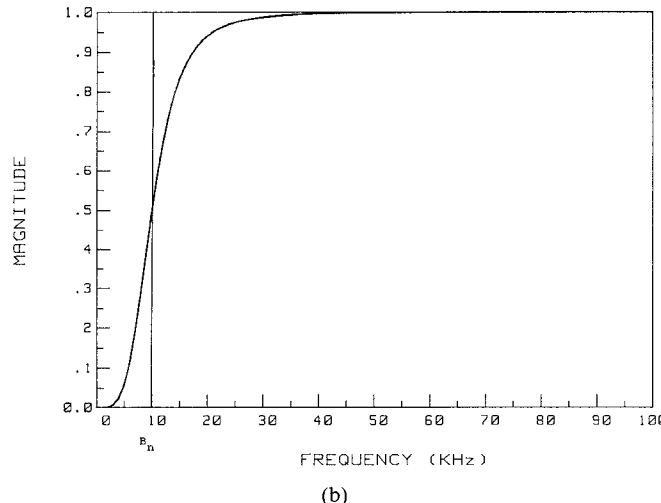
$$\varphi(t) = \tan^{-1} \left[ \frac{\hat{\theta}_e(t)}{\theta_e(t)} \right]$$

$\hat{\theta}_e(t)$  being the Hilbert transform of  $\theta_e(t)$ , defined by [3]

$$\hat{\theta}_e(t) = \frac{1}{\pi} \int_{-\infty}^{+\infty} \frac{\theta_e(\lambda)}{t - \lambda} d\lambda$$



(a)



(b)

Fig. 4. Squared modulus of the transfer functions of a second-order PLL. (a)  $H(s)$ . (b)  $H_e(s)$ .

or by its spectrum:

$$\hat{\Theta}_e(f) = -j \operatorname{sgn}(f) \Theta_e(f).$$

The instantaneous frequency of  $\varphi(t)$  can be obtained from the following expression:

$$\begin{aligned} \omega_i(t) &= \frac{d\varphi(t)}{dt} = \frac{d}{dt} \left[ \tan^{-1} \frac{\hat{\theta}_e(t)}{\theta_e(t)} \right] = \frac{\theta_e(t) \hat{\theta}'_e(t) - \hat{\theta}_e(t) \theta'_e(t)}{\theta_e^2(t) + \hat{\theta}_e^2(t)} \\ \omega_i(t) &= \frac{\theta_e(t) \hat{\theta}'_e(t) - \hat{\theta}_e(t) \theta'_e(t)}{A^2(t)} = \omega_0 + \frac{d}{dt} \phi(t) \end{aligned}$$

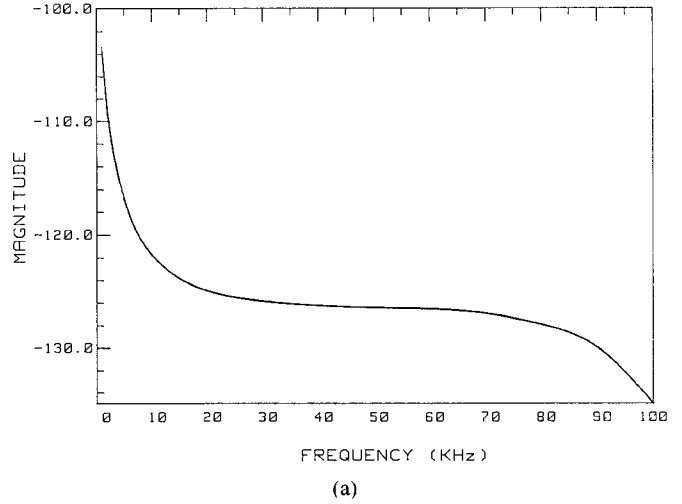
where  $\omega_0$  has to be chosen as the average value of the instantaneous frequency  $\omega_i(t)$ , that is,

$$\omega_0 = \lim_{T \rightarrow \infty} \frac{1}{T} \int_{-T/2}^{+T/2} \frac{\theta_e(t) \hat{\theta}'_e(t) - \hat{\theta}_e(t) \theta'_e(t)}{A^2(t)} dt.$$

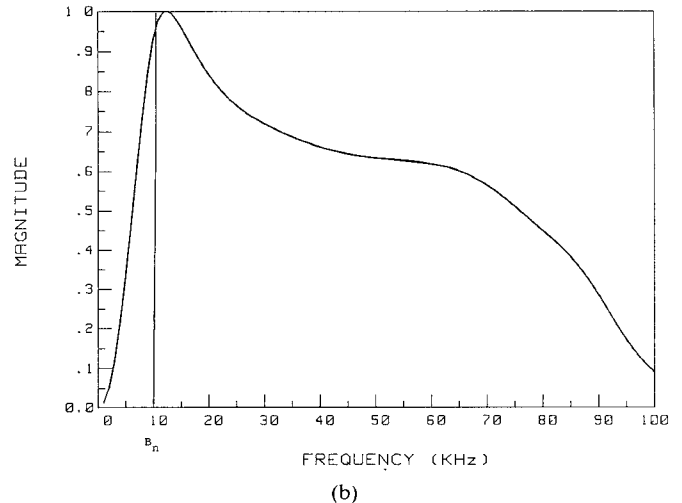
An alternative way to compute  $\omega_0$  is as the weighted average value of the power spectrum of  $\theta_e(t)$  in the following way [4]:

$$\omega_0 = \frac{\int_0^\infty f |\Theta_e(f)|^2 df}{\int_0^\infty |\Theta_e(f)|^2 df}.$$

The power spectral density of the phase error signal  $\theta_e$  has been computed for the secondary PLL values given before by



(a)



(b)

Fig. 5. Typical X-band oscillator. (a) Phase noise plot. (b) Power spectrum of the error signal  $\theta_e$ .

multiplying the curves in Figs. (4b) and (5a), thereby obtaining the plot of Fig. 5b, which shows a bandpass noise signal behavior peaked at 13 kHz, with an average frequency of 43.4 kHz, computed using the last formula.

When the main (microwave) PLL is unlocked, the signal appearing at the phase detector output is a beat between the frequencies of the VCO and the reference, its frequency range being related to the PLL's lock-in and hold-in ranges. Namely, its minimum frequency beat corresponds to the lock-in value, and its maximum value depends on the maximum frequency distance between the VCO signal and the reference. This situation is summarized in Table I.

The lock-in range can be obtained with good approximation from the formula  $\Delta\omega_L = \pm K_d K_v F(\infty)$  [1].

The information on the lock condition is detected by the presence of a beat signal at the phase detector output.

Following these criteria, a circuit capable of making a distinction between both situations has been developed; it works as a PM demodulator of the phase detector output signal and gives as a result a LED indication and a TTL logic level.

### III. EXPERIMENTAL SETUP

A practical circuit (Fig. 6) has been built to be used as a lock indicator in a  $\times 3$  (9 to 27 GHz) PLL frequency multiplier [5] in which the phase detection was made at 27 GHz. The signal

TABLE I

PLL(main)	Phase detector output
Locked	Band-pass noise signal
Unlocked	Beat (difference of frequencies) * minimum: lock-in limit * maximum: $ VCO - Reference _{max}$

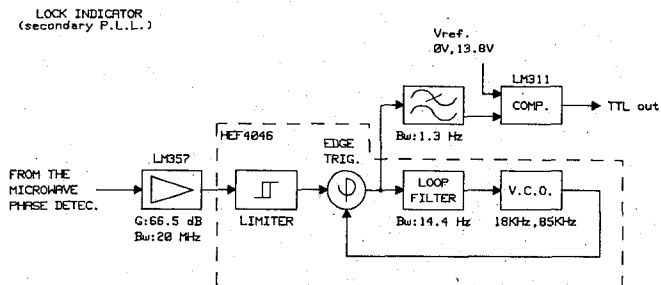


Fig. 6. Block diagram of the practical lock indicator circuit.

coming from the microwave phase detector is fed, after amplification, to a HEF4046 PLL circuit, which contains limiter, phase detector, and VCO.

As phase detector, an edge-controlled digital memory network, which is sensitive to phase and frequency and is preceded by a limiter, is used. This guarantees that the (secondary) VCO control signal is kept at a high level even if the secondary PLL is not locked to the beat signal coming from the microwave phase detector.

The VCO frequency spans a range from a value greater than the lock-in range down to a value lower than the cutoff frequency  $B_n$ , where both quantities refer to the main loop.

When the main PLL is out of lock, the secondary loop tries to lock to the beat signal, bringing the VCO control signal to a high level. However, under locked conditions in the main loop, the secondary loop keeps the VCO frequency around the average frequency value of the  $\Theta_e$  spectrum. The fast variations are not tracked given the narrow bandwidth chosen for the PLL; therefore, the VCO control signal now takes a lower level than before. Feeding this VCO control signal to a comparator after smoothing (narrow-band low-pass filtering), a digital level corresponding to the lock condition in the main PLL is obtained in a very easy way.

The main characteristics of this circuit are the following:

#### Amplifier:

- \* Gain: 66.5 dB
- \* Bandwidth: 20 MHz

#### PLL:

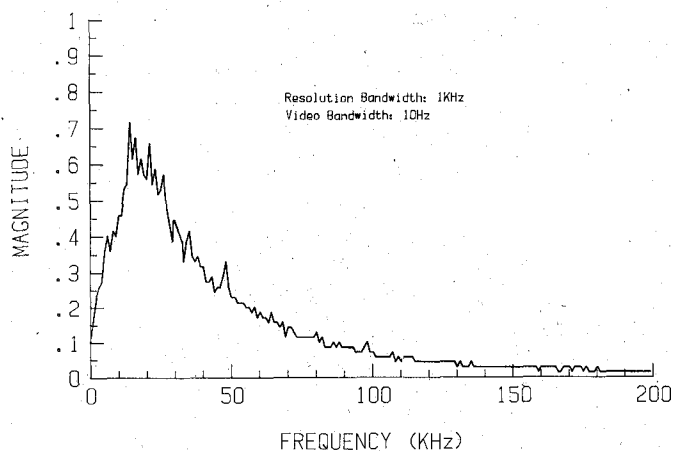
- \* VCO swing: 18 kHz to 85 kHz
- \* Phase detector output swing: 0 V to 13 V
- \* Loop filter bandwidth: 14.4 Hz

#### Comparator:

- \* Smoothing filter bandwidth: 1.3 Hz
- \* Voltage reference swing: 13.8 V to 0 V
- \* TTL output: LOCKED  $\rightarrow$  "0"
- UNLOCKED  $\rightarrow$  "1"

This circuit has been used also with success in other microwave phase locked oscillators, where the phase detection was made at

SPECTRUM OF THE INPUT SIGNAL

Fig. 7. Spectrum of the input signal  $\theta_e$  to the lock indicator circuit.

SECONDARY P. L. L. RESPONSE

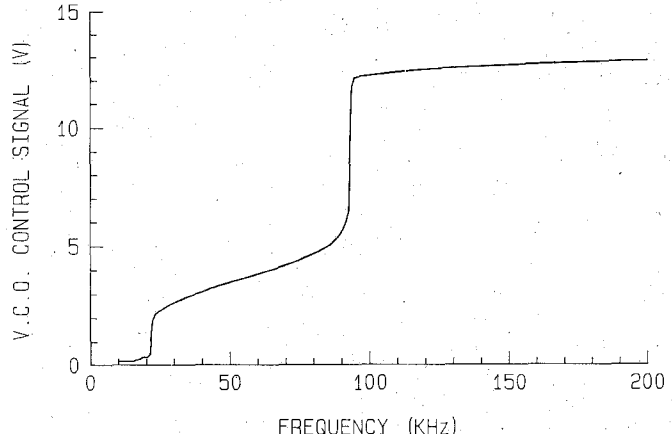


Fig. 8. VCO control signal of the lock indicator circuit versus the input frequency.

29.7 GHz, 2.55 GHz, and 290 MHz, without changes other than the threshold level for each PLO.

Fig. 7 shows the measured spectrum of the input signal to the secondary PLL. It corresponds to the phase detector output of a  $\times 3$  frequency multiplier which synthesizes a 27.03 GHz signal from a 9.01 GHz reference, with a cutoff frequency of 20 kHz, a damping coefficient of 1.14, and a lock-in limit of  $\pm 277.7$  kHz. Its average frequency has been calculated to be a 73 kHz.

Introducing it in the secondary PLL the average value of the VCO control signal takes a 3.8 V value, which corresponds to 70 kHz frequency, in agreement with the theoretical value obtained. By adjusting the threshold reference level to 4.4 V for proper operation, all input frequencies above 100 kHz will be considered beat signals, denoting an unlocked condition in the main PLL. Fig. 8 shows the VCO control signal versus the input frequency of this secondary PLL.

#### IV. CONCLUSIONS

A new electronic circuit which performs a lock indication in microwave PLL's has been presented. It does not make use of the known quadrature phase detector method, reducing in this way the cost and complexity of the microwave circuitry. A

frequency-voltage conversion is made in a secondary low-frequency PLL such that the phase detector output of the microwave PLL gives, in a logic level format, an indication of the lock condition in the main PLL.

This circuit has been used with success in microwave PLO's in which the phase detection was made at 290 MHz, 2.55 GHz, 27 GHz, and 29.7 GHz.

#### REFERENCES

- [1] F. M. Gardner, *Phaselock Techniques*. New York: Wiley, 1979
- [2] W. P. Robins, *Phase Noise in Signal Sources* (IEE Telecommunications Series 9). London: Peter Peregrinus Ltd., 1982
- [3] A. B. Carlson, *Communication Systems*. New York: McGraw-Hill, 1975
- [4] L. E. Franks, *Signal Theory*. Englewood Cliffs, NJ: Prentice Hall, 1975
- [5] J. Berenguer, J. Bara, and A. Comeron, "Compact and simple  $\times 3$  (9 to 27 GHz) PLL frequency multiplier using harmonic phase detection," in *Proc. 41st Ann. Symp. Frequency Control* (Philadelphia), May 1987, pp. 492-494.

### Polarization Effects on Microwave Imaging of Dielectric Cylinder

TAH-HSIUNG CHU, MEMBER, IEEE

**Abstract**—In this paper, theoretical and experimental studies of frequency-swept microwave imaging of an infinitely long lossless homogeneous dielectric cylinder illuminated by a right-hand circularly polarized (RHCP) plane wave are presented. The reconstructed polarization-dependent microwave image can be seen as embodying contributions from specular, axial, glory, and stationary ray components of the scattered field of the selected receiving polarization state. An automated microwave imaging system employing frequency and polarization diversity techniques is utilized to verify the theoretical and numerical results.

#### I. INTRODUCTION

Frequency-swept microwave imaging of dielectric objects satisfying the Born approximation has been shown to be a cost-effective tool in nondestructive evaluation [1]. The polarization effect on the reconstructed microwave image is negligible when the dielectric object is weakly scattering. However, as the product of object radius in wavelength and the change in object refraction index from its surrounding medium becomes greater than 0.175, the Born approximation fails [2]; hence the polarization states of the illuminating and receiving fields must be taken into consideration. In this paper, theoretical and experimental studies of the polarization effects on the frequency-swept microwave image of an infinitely long dielectric cylinder not satisfying the Born approximation are presented.

#### II. THEORETICAL CONSIDERATIONS

Consider an infinitely long homogeneous nondispersive dielectric cylinder with relative dielectric constant  $\epsilon$ , and radius  $a$  in a backscattering arrangement as shown in Fig. 1 being illuminated by a right-hand circularly polarized (RHCP) plane wave  $\vec{E}'_R$  expressed as

$$\vec{E}'_R = \frac{1}{\sqrt{2}} (E'_\phi \hat{\phi} - E'_z \hat{z}) = \frac{1}{\sqrt{2}} E_0 e^{-jkR} (\hat{\phi} - j\hat{z}) \quad (1)$$

Manuscript received January 25, 1988; revised April 28, 1988.

The author is with the Department of Electrical Engineering, National Taiwan University, Taipei, Taiwan, R.O.C.

IEEE Log Number 8822155

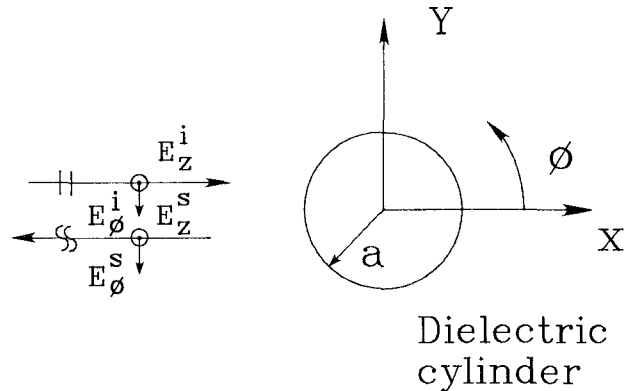


Fig. 1 The scattering geometry

where  $\exp(j\omega t)$  is implied. In the following, linearly polarized scattered field components and their reconstructed images will be discussed first. Results are then extended to the circular polarization case.

The scattered far fields for each linear polarization state in the resonance and high-frequency regions ( $ka > 1$ ) can be characterized by rays using a modified geometrical optics method [3]–[5], and they are given as

$$E_\phi^s = E_0 \sqrt{\frac{a}{2R}} e^{jkR} \cdot \left[ f_0 e^{j\theta_0} + \sum_l f_{A_l} e^{j\theta_{A_l}} + \sum_m f_{G_m} e^{j\theta_{G_m}} + \sum_n f_{S_n} e^{j\theta_{S_n}} \right] \quad (2)$$

and

$$E_z^s = E_0 \sqrt{\frac{a}{2R}} e^{jkR} \cdot \left[ g_0 e^{j\psi_0} + \sum_l g_{A_l} e^{j\psi_{A_l}} + \sum_m g_{G_m} e^{j\psi_{G_m}} + \sum_n g_{S_n} e^{j\psi_{S_n}} \right]. \quad (3)$$

Equations (2) and (3) show that the backscattered fields for each linear polarization state are superpositions of various ray components. The first term is the specular ray. The terms with subscripts  $A$ ,  $G$ , and  $S$  are axial, glory, and stationary rays and  $l$ ,  $m$ , and  $n$  are numbers of internal reflection for each ray component inside the dielectric cylinder as described in [3]–[5]. For example,  $f_{A_l}$  and  $\theta_{A_l}$  are the amplitude and phase of the single bounce axial ray component in the  $E_\phi^s$  field. The various ray amplitudes are related to the cylinder radius, dielectric constant, and radius of curvature of the emerging ray phase front after interaction with the cylinder surface, and the ray phases are equal to the product of the wavenumber  $k$  and the optical length of a given ray between entrance and emergence. They are polarization dependent and are given in [4] and [5].

Since the phase term for each ray component is linearly proportional to the optical length it travels, one-dimensional Fourier inversion of the scattered far field acquired using the frequency diversity technique (i.e., varying the wavenumber  $k$ ) gives a range profile of the illuminated cylinder for each selected